DC2 and KCP2 mediate the interaction between the oligosaccharyltransferase and the ER translocon

Shiteshu Shrimal, Natalia A. Cherepanova, and Reid Gilmore

Department of Biochemistry and Molecular Pharmacology, University of Massachusetts Medical School, Worcester, MA

In metazoan organisms, the STT3A isoform of the oligosaccharyltransferase is localized adjacent to the protein translocation channel to catalyze co-translational N-linked glycosylation of proteins in the endoplasmic reticulum. The mechanism responsible for the interaction between the STT3A complex and the translocation channel has not been addressed. Using genetically modified human cells that are deficient in DC2 or KCP2 proteins, we show that loss of DC2 causes a defect in co-translational N-glycosylation of proteins that mimics an *STT3A*$^{-/-}$ phenotype. Biochemical analysis showed that DC2 and KCP2 are responsible for mediating the interaction between the protein translocation channel and the STT3A complex. Importantly, DC2- and KCP2-deficient STT3A complexes are stable and enzymatically active. Deletion mutagenesis revealed that a conserved motif in the C-terminal tail of DC2 is critical for assembly into the STT3A complex, whereas the lumenal loop and the N-terminal cytoplasmic segment are necessary for the functional interaction between the STT3A and Sec61 complexes.

Introduction

Asparagine-linked glycosylation is an essential protein modification reaction critical for the folding, trafficking, and function of many proteins that enter the secretory pathway. In most eukaryotes, the oligosaccharyltransferase (OST) complex is composed of a catalytic subunit (an STT3 protein) plus as many as eight accessory subunits. Plant and metazoan organisms encode two STT3 proteins (STT3A and STT3B) that are assembled with a set of six shared OST subunits (ribophorins I and 2, OST48, DAD1, OST4, and TMEM258). An oxidoreductase, either MagT1 or TUSC3, is assembled with STT3B as a complex-specific accessory subunit (Cherepanova et al., 2014; Cherepanova and Gilmore, 2016). DC2 (*OSTC* gene) and KCP2, two small membrane proteins, were initially detected as novel OST subunits in translocation channel–associated OST complexes (Shibatani et al., 2005). STT3A complexes interact with the protein translocation channel (Shibatani et al., 2005; Ruiz-Canada et al., 2009) and mediate co-translational N-glycosylation when the acceptor site (NXT/S/C, sequon) is positioned ∼65–75 residues from the peptidyltransferase site on the ribosome (Whitley et al., 1996; Nilsson et al., 2003).

The STT3A and STT3B complexes have complementary roles in N-linked glycosylation. Depletion of STT3A by siRNA treatment or knockout of *STT3A* by CRISPR/Cas9 gene editing causes hypoglycosylation of proteins, resulting in induction of the unfolded protein response (UPR) pathway (Ruiz-Canada et al., 2009; Cherepanova and Gilmore, 2016). The STT3B complex can mediate posttranslocational glycosylation of acceptor sites that have been skipped by the STT3A complex, including sequons that are located in the last 65 residues of the protein (Shrimal et al., 2013b). Co-translational glycosylation by the STT3A complex is responsible for the modification of the majority of the sequons in the glycoproteome; hence, depletion of STT3B or disruption of the *STT3B* gene causes little or no induction of the UPR pathway (Ruiz-Canada et al., 2009; Cherepanova and Gilmore, 2016). A co-translational scanning mechanism enhances glycosylation efficiency because acceptor sites in folded polypeptides do not have access to the catalytic site in STT3 proteins, as revealed by the structures of the eubacterial and archaebacterial STT3 homologues PglB and AglB (Lizak et al., 2011; Matsumoto et al., 2013).

The mechanism responsible for localization of the STT3A complex adjacent to the protein translocation channel has not been addressed at either a biochemical or structural level. The shared OST subunits are unlikely to contribute to localization, as their presence in both complexes would result in competition between STT3A and STT3B for the Sec61-proximal location. One hypothesis would be that the STT3 proteins, which are only 59% identical in sequence, contain segments that either promote for STT3A, or prevent for STT3B, a stable interaction with the protein translocation channel. Alternatively, the DC2 or KCP2 proteins might mediate the interaction with the Sec61

Correspondence to Reid Gilmore: reid.gilmore@umassmed.edu

Abbreviations used: BN, blue native; CDG, congenital disorders of glycosylation; CL, cleared lysate; co-IP, coimmunoprecipitation; Dol-PP-OS, dolichol-linked oligosaccharide; OST, oligosaccharyltransferase; pGran, progranulin; PIC, protease inhibitor cocktail; pSAP, prosaposin; RAMP, ribosome-associated membrane protein; RIPA, radioimmunoprecipitation analysis; sgRNA, single-guide RNA; SHBG, sex hormone–binding globulin; Tf, transferrin; TM, transmembrane; UPR, unfolded protein response.

The Rockefeller University Press
J. Cell Biol. Vol. 216 No. 11 3625–3638
https://doi.org/10.1083/jcb.201702159

complex. However, it has been reported that DC2 is present in both the STT3A and STT3B complexes (Roboti and High, 2012a), whereas KCP2 was detected in only a subset of STT3A complexes (Roboti and High, 2012b). If either conclusion can be confirmed, DC2 and KCP2 would lack the specificity to localize the STT3A complex adjacent to the Sec61 complex. A third hypothesis is that translocation channel–associated proteins including the STT3A complex are not recruited until the nascent polypeptide is exposed in the lumen of the rough ER (Conti et al., 2015). Cryoelectron tomographic analysis of canine microsomes revealed a population of ribosome-Sec61 complexes that lack an associated OST complex (Pfeffer et al., 2014). One argument against the recruitment hypothesis is that glycosylation of a nascent polypeptide occurs by an N-terminal to C-terminal scanning mechanism in a highly synchronized manner (Chen et al., 1995; Shrimal and Gilmore, 2013).

Here, we have analyzed the functional association between the STT3A complex and the protein translocation channel using human embryonic kidney–derived cell lines (HEK293) that were genetically modified to not express STT3A, DC2, or KCP2. KCP2 is unstable in *DC2*$^{-/-}$ cells, whereas both DC2 and KCP2 are unstable in *STT3A*$^{-/-}$ cells, demonstrating that DC2 and KCP2 are exclusive accessory subunits of the STT3A complex. Inactivation of the *KCP2* gene causes a partial reduction in glycosylation of STT3A-specific substrate prosaposin (pSAP), consistent with the results reported previously using an siRNA knockdown approach (Roboti and High, 2012b). In marked contrast, *DC2*$^{-/-}$ cells have a severe defect in glycosylation of STT3A substrates that phenocopies loss of the STT3A protein. STT3A complexes that lack DC2 or KCP2 are enzymatically active when assayed using a synthetic peptide acceptor but do not form stable complexes with the Sec61 complex. Deletion mutagenesis revealed that lumenally exposed domains of DC2 are necessary for incorporation into the STT3A complex and are important for the functional interaction between the STT3A complex and the Sec61 complex.

Results

DC2 and KCP2 are subunits of the STT3A complex

The CRISPR/Cas9 gene-editing system was used to generate HEK293-derived cell lines that do not express DC2 or KCP2. Two CRISPR targets were selected in the *DC2* and *KCP2* genes (Table S1). Protein immunoblots using antisera specific for DC2 or KCP2 were used as a primary screen to select cell clones that do not express DC2 or KCP2. Sequencing of the PCR amplicons flanking the DC2 target site revealed three amplification products (Fig. S1 A) with insertions of 1, 2, or 78 bp relative to the WT sequence. The genome of HEK293 cells contains three copies of the *DC2* gene and two copies of the *KCP2* gene, as HEK293 cells are hypotriploid (Lin et al., 2014). Sequencing of DNA flanking the *KCP2* target site revealed a single amplification product containing a 1-bp insertion (Fig. S1 A). Analysis of the three most probable off-target sites for each single-guide RNA (sgRNA; Table S1) did not disclose indel mutations (Fig. S1 B).

Total cell extracts were resolved by SDS-PAGE for protein immunoblot analysis using antibodies specific for several OST subunits, a gel loading control (GAPDH), and three ER-resident proteins (BiP, Sec61α, and malectin; Fig. 1 A). STT3A and STT3B are undetectable by protein immunoblot analysis in the *STT3A*$^{-/-}$ and *STT3B*$^{-/-}$ cell lines, as reported previously (Cherepanova and Gilmore, 2016). Cells lacking STT3B show slightly elevated expression of STT3A but do not show a reduction in expression of ribophorin I or KCP2. In contrast, *STT3A*$^{-/-}$ cells lack detectable expression of DC2 and KCP2. A reduction in KCP2 content had been reported previously in cells that were treated with an *STT3A* siRNA but not with an *STT3B* siRNA (Roboti and High, 2012b). The antisera to DC2 recognizes a faint nonspecific protein with a mobility slightly slower than DC2 in the *DC2*$^{-/-}$ and *STT3A*$^{-/-}$ cell lines. The *DC2*$^{-/-}$ cells express STT3A, but KCP2 is absent. The *KCP2*$^{-/-}$ cell line retains normal expression of STT3B, ribophorin I, and malectin but has slightly reduced expression of STT3A and DC2. This hierarchy of stable expression of STT3A, DC2, and KCP2 indicates that DC2 and KCP2 are obligate subunits of the STT3A complex. Given that KCP2 is unstable in *DC2*$^{-/-}$ cells, DC2 likely provides the binding site for KCP2 on the STT3A complex. Coimmunoprecipitation (co-IP) experiments conducted using radioimmunoprecipitation analysis (RIPA) lysis and wash buffers revealed that HA-DC2 interacts with untagged KCP2 when these OST subunits are overexpressed in *DC2*$^{-/-}$ cells (Fig. S2 A). The intact STT3A complex is not stable in RIPA buffer.

Reduction in the cellular content of STT3A, whether achieved by siRNA treatment (Ruiz-Canada et al., 2009) or CRISPR/Cas9 gene editing (Cherepanova and Gilmore, 2016), causes an induction of the UPR pathway as detected by elevated expression of the ER chaperone BiP. BiP protein levels also increase in *DC2*$^{-/-}$ cells but not in *KCP2*$^{-/-}$ cells, indicating that loss of DC2 has a greater impact than loss of KCP2 on accumulation of unfolded proteins in the ER lumen.

Previous attempts to determine which OST complexes contain KCP2 as a subunit were technically challenging because of the incomplete depletion of KCP2 that can be achieved in siRNA-treated cells (Roboti and High, 2012b). Blue native PAGE (BN-PAGE) of digitonin lysates of HeLa or HepG2 cells (Roboti and High, 2012a,b) or CHO cells (Shrimal and Gilmore, 2015) resolves the OST into two STT3A complexes (470- and 500-kD complexes; Fig. 1, arrowheads 1 and 2) and a diffusely migrating 550-kD STT3B complex (Fig. 1 B, arrowhead 3). The mobility of membrane protein complexes relative to molecular weight markers on BN-PAGE gels is influenced by protein molecular weight, shape, charge, and protein-bound detergent, so we refer to these complexes by the apparent molecular weights that were assigned previously (Roboti and High, 2012a,b). Antisera that recognize DC2 or KCP2 did not detect a specific band in the vicinity of the STT3B complex when extracts from WT cells were analyzed, indicating that neither protein is a subunit of the STT3B complex. Moreover, the mobility of the STT3B complex did not increase in extracts prepared from the *DC2*$^{-/-}$ and *KCP2*$^{-/-}$ cells. If the absence of KCP2 accounts for the more rapid mobility of the 470-kD complex (Roboti and High, 2012a), STT3A complexes prepared from *KCP2*$^{-/-}$ cells should migrate at the band 1 position (470 kD). Instead, two STT3A and DC2 immunoreactive complexes were detected, both of which showed increased mobility relative to WT STT3A complexes (Fig. 1 B, arrowheads 1a and 2a). Assembly of KCP2 into both STT3A complexes was confirmed by probing BN-PAGE blots with anti-KCP2 sera. STT3A complexes from *DC2*$^{-/-}$ cells showed an additional slight increase in mobility

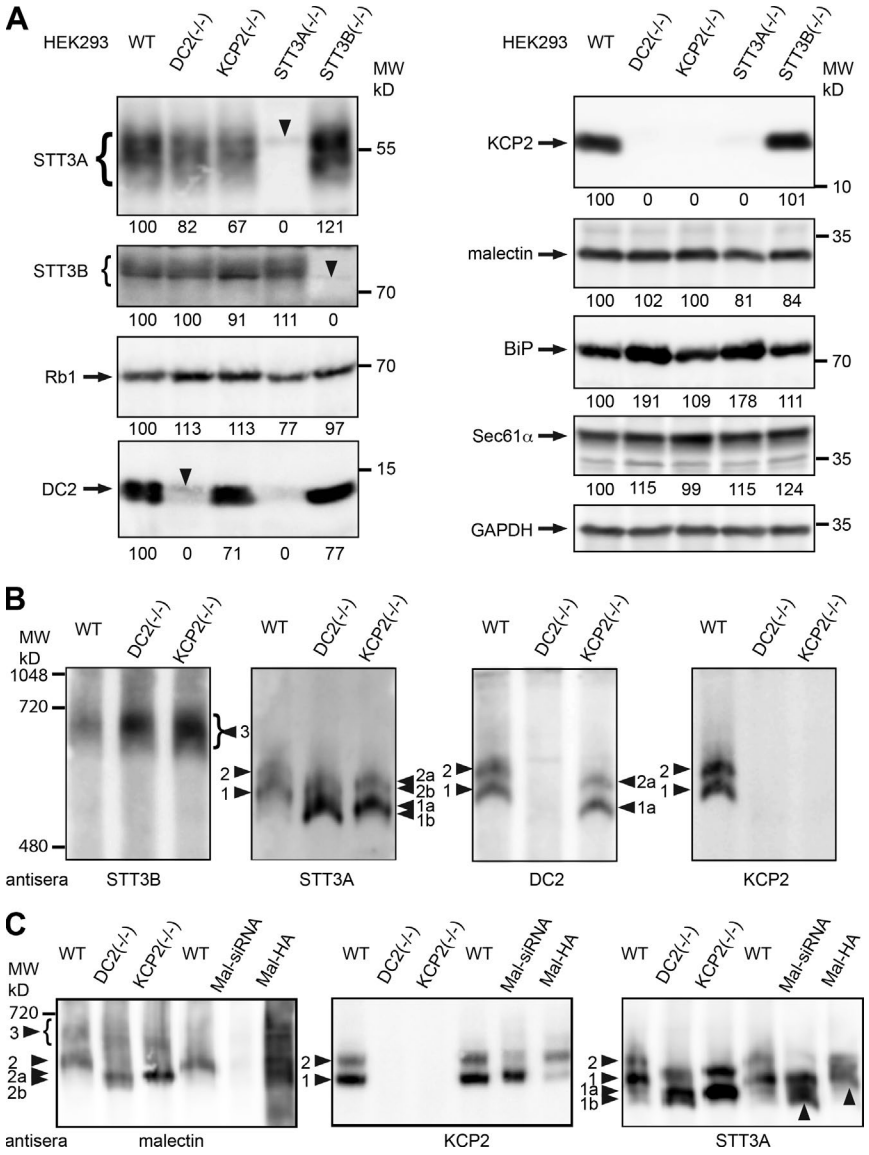

Figure 1. **Protein immunoblot analysis of HEK293-derived cell lines.** (A) Total protein extracts (100 µg) from cells were resolved by SDS-PAGE and analyzed on protein immunoblots using the specified antisera. GAPDH served as a gel loading control. Downward-pointing arrowheads indicate nonspecific background bands. Quantified values below gel lanes are the mean of two or more experiments. (B and C) BN-PAGE of digitonin extracts of WT, *DC2*$^{-/-}$, and *KCP2*$^{-/-}$ HEK293 cells. (C) As indicated, WT cells were either treated with malectin siRNA (mal-siRNA) for 72 h or malectin-HA was overexpressed for 24 h (Mal-HA). OST complexes were detected by immunoblotting with the specified antisera. Labeled arrowheads designate the following protein complexes: 1, 470-kD STT3A complex; 2, 500-kD STT3A complex; 3, 550-kD STT3B complex; 1a and 2a, STT3A complexes lacking KCP2; 1b and 2b, STT3A complexes lacking DC2 and KCP2.

consistent with the complete absence of both DC2 and KCP2 (Fig. 1 B, arrowheads 1b and 2b).

Because both the 470- and 500-kD complexes contain DC2 and KCP2, what protein could account for the decreased mobility of the 500-kD complex? Malectin, an ER lectin that binds the Glc α-1,3 Glc disaccharide (Schallus et al., 2008, 2010), coimmunopurifies with the STT3A and STT3B complexes (Cherepanova et al., 2014) via an interaction with ribophorin I (Qin et al., 2012). Blotting with an antibody specific for malectin resulted in detection of the 500-kD STT3A complex and the 550-kD STT3B complex, but not the 470-kD complex (Fig. 1 C, arrowheads 2 and 3). STT3A complexes lacking KCP2 or both KCP2 and DC2 were also recognized by the anti-malectin sera (Fig. 1 C, arrowheads 2a and 2b). Modulation of malectin protein expression levels by siRNA treatment or malectin-HA overexpression (Fig. S2 B) respectively reduced or enhanced the malectin immunoblot signal in the vicinity of the STT3A and STT3B complexes (Fig. 1 C). Importantly, reducing or increasing malectin expression altered the ratio of the 470- and 500-kD complexes as detected using the anti-KCP2 sera (Fig. 1 C). Although this conclusion was confirmed using anti-STT3A sera, perturbation of malectin expression appeared to increase the recovery of KCP2-deficient STT3A complexes, for unknown reasons (Fig. 1 C, upward pointing arrowheads). We conclude that malectin is a substoichiometric subunit of the OST in HEK293 cells, being present in ∼50% of the STT3A complexes and an indeterminate fraction of the STT3B complexes. BN-PAGE immunoblots of six mammalian cell lines showed that KCP2 was present in both complexes in all tested cell lines (Fig. S2 C). Moreover, cell lines that had less intense anti-malectin immunoblot signals were enriched in the 470-kD complex relative to the 500-kD complex.

DC2 is required for efficient glycosylation of STT3A-dependent substrates

DC2 and KCP2 are low molecular weight membrane proteins that have three (DC2) or four (KCP2) hydrophobic segments that are sufficiently long to span a membrane (Shibatani et al., 2005). Analysis of the human DC2 and KCP2 sequences using the TOPCONS (http://dgpred.cbr.su.se) and TMHMM (www.cbs.dtu.dk/services/TMHMM-2.0) webservers predicted a three-transmembrane (3TM; N_{cyt}-C_{lum}) topology for DC2 and a 4TM (N_{cyt}-C_{cyt}) topology for KCP2 (Fig. 2 A). Glycosylation acceptor sites inserted into the predicted lumenal loop of DC2

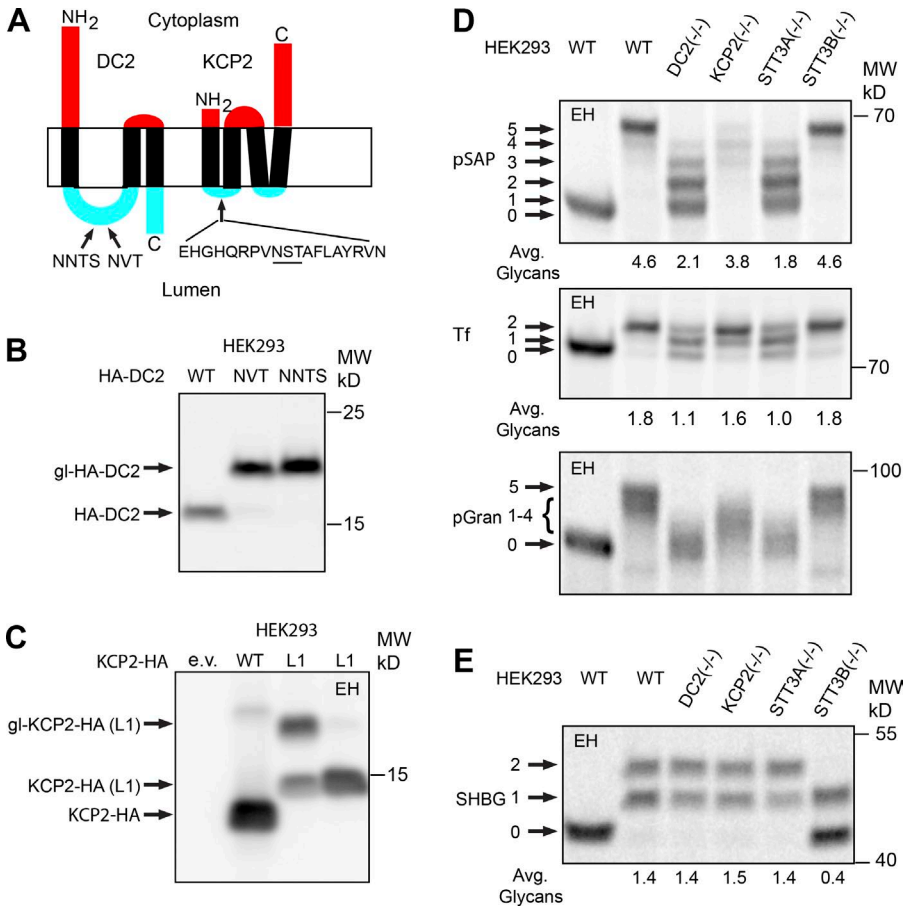

Figure 2. **Protein glycosylation in OST mutant cell lines.** (A) Protein topology models for DC2 and KCP2 showing the location of inserted glycosylation sites. (B–E) WT and mutant cell lines were transfected with the following expression vectors: B, HA-DC2, HA-DC2 NVT, or HA-DC2 NNTS; C, WT KCP2-HA, KCP2-HA L1, or empty vector (e.v.); D, Tf-DDKHis; and E, SHBG. (D) pSAP and pGran are endogenous proteins. (B and C) 100 µg cell lysate was immunoblotted with anti-HA antibody to detect nonglycosylated (HA-DC2, KCP2-HA, and KCP2-HA L1) and glycosylated (gl-HA-DC2 and gl-KCP2-HA L1) proteins. (D and E) Cells were pulse-labeled or pulse-chase labeled as described in Materials and Methods. The glycoprotein substrates were precipitated with anti-SapD, anti-DDK for Tf-DDKHis, anti-Gran, or anti-SHBG sera and then resolved by SDS-PAGE. (C–E) EH designates treatment with endoglycosidase H. Quantified values below gel lanes (D and E) are the mean number of glycans per protein chain as determined from two or more experiments. Numbered arrows (D and E) designate the number of N-linked glycans.

(Fig. 2 A) were modified in vivo (Fig. 2 B), confirming the predicted protein orientation. Protease digestion experiments using intact microsomes had shown that the C terminus of FLAG-KCP2 is trypsin sensitive, whereas an N-terminal FLAG tag is trypsin resistant, thereby supporting a 3TM N_{lum}-C_{cyt} topology (Roboti and High, 2012a). Because this topology would necessitate an unusually long third TM span (~40 residues), we decided to test whether the loop between the first two TM spans (L1) is exposed to the lumen or the cytosol by inserting a peptide containing a glycosylation acceptor site (NST) into KCP2-HA (Fig. 2 A). The expanded loop satisfies the minimal distance requirement of 12–14 residues between a glycosylation acceptor site and the lumenal ER surface (Nilsson and von Heijne, 1993; Cheung and Reithmeier, 2007). Although KCP2-HA migrates as a single band of ~15 kD, there are two forms of KCP2-HA L1 that differ by ~3 kD (Fig. 2 C). The less rapidly migrating band was sensitive to endoglycosidase H digestion consistent with localization of L1 in the ER lumen, thereby supporting the 4TM N_{cyt}-C_{cyt} topology model. The trypsin insensitivity of the FLAG-KCP2 construct (Roboti and High, 2012a) is likely explained by the close proximity of the tag to the membrane surface and the presence of multiple aspartate residues in the FLAG tag (DYKDDDDK) that bias against cleavage at nearby lysine residues (Siepen et al., 2007).

We next asked whether the absence of DC2 or KCP2 reduced the glycosylation of pSAP, transferrin (Tf), and progranulin (pGran), three proteins that are well-characterized substrates of the STT3A complex (Ruiz-Canada et al., 2009; Shrimal et al., 2013a,b). pSAP has five glycosylation acceptor sites that are efficiently modified in WT or *STT3B*$^{-/-}$ cells. Elimination of the STT3A complex results in the synthesis of pSAP glycoforms that on average lack three of the five glycans (Fig. 2 D). The *DC2*$^{-/-}$ cells displayed the same pattern of pSAP hypoglycosylation as *STT3A*$^{-/-}$ cells. *KCP2*$^{-/-}$ cells had a detectable, but much less severe, defect in pSAP glycosylation, consistent with previous results obtained by siRNA-mediated knockdown of KCP2 (Roboti and High, 2012b). The major glycoform of Tf synthesized by the WT and *STT3B*$^{-/-}$ cells is glycosylated on both acceptor sites. Cells lacking the complete STT3A complex or DC2 synthesize Tf lacking one glycan (Fig. 2 D). Although the resolution of pGran glycoforms is not sufficient for quantification, the DC2-deficient cells had a glycosylation defect that phenocopied loss of the entire STT3A complex. As observed for pSAP and Tf glycosylation, the *KCP2*$^{-/-}$ cells had a less severe defect in pGran glycosylation.

To rule out the possibility that loss of DC2 or KCP2 causes a general defect in N-glycosylation, we examined glycosylation of the STT3B substrate sex hormone–binding globulin (SHBG), a protein that has two extreme C-terminal glycosylation sites (Shrimal et al., 2013b; Cherepanova and Gilmore, 2016). Glycosylation of SHBG was not reduced in *STT3A*$^{-/-}$, *DC2*$^{-/-}$, or *KCP2*$^{-/-}$ cells but was severely reduced in *STT3B*$^{-/-}$ cells, providing further evidence that DC2 and KCP2 are not subunits of the STT3B complex (Fig. 2 E).

DC2 and KCP2 are necessary for substrate accessibility, not enzymatic activity

Multiple lines of evidence indicate that STT3 proteins are the catalytic subunits of eukaryotic OSTs (Wacker et al., 2002; Yan and Lennarz, 2002; Kelleher et al., 2003). We next asked

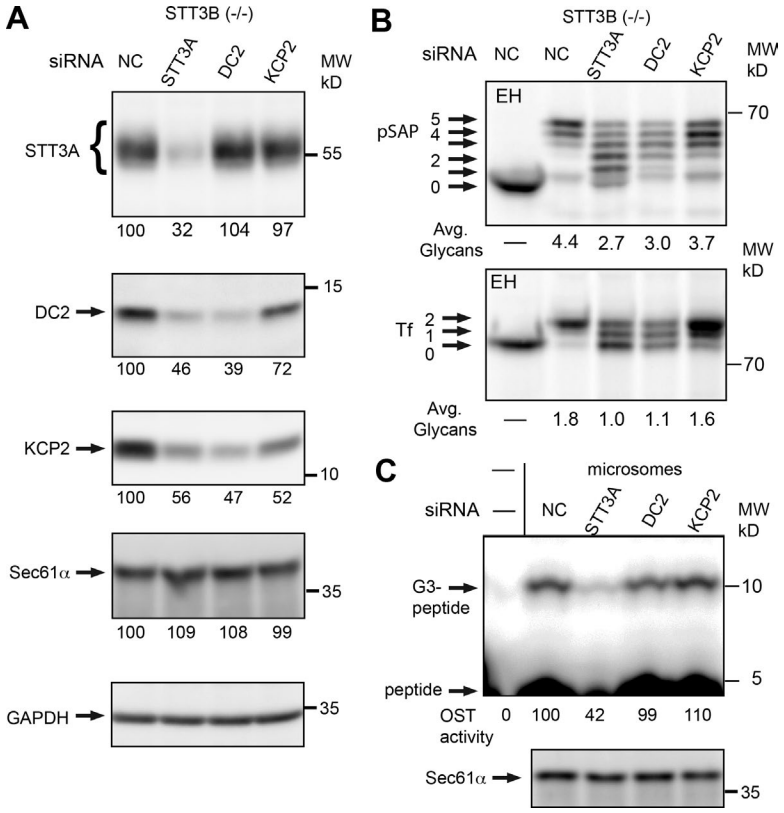

Figure 3. **OST assays of microsomes isolated from siRNA-treated *STT3B*$^{-/-}$ cells.** *STT3B*$^{-/-}$ cells were treated with a negative control siRNA (NC) or siRNAs specific for STT3A, DC2, or KCP2. (A) Cell extracts were resolved by SDS-PAGE for protein immunoblot analysis. (B) After 48 h of siRNA treatment, cells were retransfected with the siRNA plus pSAP-DDKHis or Tf-DDKHis expression vectors. After 24 h, pulse-labeled proteins were immunoprecipitated using anti-DDK sera. EH, endoglycosidase H. Numbered arrows designate the number of N-linked glycans. (C) A buffer control (–) or solubilized HEK293-derived microsomes were assayed for OST activity using bovine Dol-PP-OS as the donor substrate and a fluorescent peptide as the acceptor substrate. The glycopeptide product (peptide-$GlcNAc_2Man_9Glc_3$, G3-peptide) was separated from the peptide by gel electrophoresis. Protein immunoblot analysis using anti-Sec61α of microsomes that were used for the OST assays. Quantified values below gel lanes are the mean of either two (A and B) or three (C) determinations.

whether the loss of DC2 or KCP2 might reduce STT3A-mediated glycosylation of a synthetic acceptor peptide in addition to reducing glycosylation of polypeptides.

Assays comparing the in vitro OST activity of microsomes isolated from WT and STT3A-, DC2-, or KCP2-deficient cell lines were difficult to interpret because of the presence of the STT3B complex (not depicted). To avoid this complication, we used siRNAs to knock down STT3A, DC2, or KCP2 in the *STT3B*$^{-/-}$ cell line (Fig. 3 A). As reported previously (Cherepanova and Gilmore, 2016), siRNA-mediated knockdown of STT3A in HEK293 cells was somewhat less effective than in HeLa cells. Nonetheless, the expression of the STT3A complex dropped roughly twofold based on the reduced immunoblot signals for STT3A, DC2, and KCP2 in the *STT3A* siRNA–treated cells. siRNA knockdown of DC2 and KCP2 also caused roughly a twofold reduction in expression of the targeted protein (Fig. 3 A). Despite the incomplete knockdown of OST subunits, we observed substantial reductions in N-glycosylation of pSAP and Tf in cells treated with the *STT3A*, *DC2*, and *KCP2* siRNAs (Fig. 3 B).

Microsomes were isolated from the siRNA-treated *STT3B*$^{-/-}$ cells, and their concentration was adjusted based on the protein immunoblot signal for the ER-localized protein Sec61α (Fig. 3 C, bottom). Digitonin-solubilized microsomes were assayed for OST activity using a fluorescent peptide as the acceptor substrate (Kohda et al., 2007) and dolichol-linked oligosaccharides (Dol-PP-OSs) isolated from bovine pancreas as the donor substrate (Fig. 3 C, top). Glycopeptide products were separated from the peptide by SDS gel electrophoresis (Gerber et al., 2013). siRNA-mediated depletion of STT3A caused a reduction in peptide N-glycosylation activity consistent with the twofold reduced expression of the STT3A complex. In marked contrast, depletion of DC2 or KCP2 did not cause a reduction in peptide glycosylation, demonstrating that these subunits are not essential for the peptide glycosylation activity of the STT3A complex. Thus, DC2 and KCP2 are necessary for glycosylation of polypeptide substrates by the STT3A complex, but not for peptide binding and catalysis.

Glycosylation sites on nascent polypeptides become accessible to the STT3A active site when the acceptor site is 65–75 residues from the peptidyltransferase site on the ribosome (Whitley et al., 1996; Kowarik et al., 2002; Nilsson et al., 2003). This short distance mandates a direct association between the protein translocation channel and the STT3A complex, which has been experimentally detected by the presence of the STT3A complex in ribosome-associated membrane protein (RAMP) fractions that are obtained by digitonin solubilization of microsomes (Shibatani et al., 2005). We measured the solubility of STT3A in digitonin-NaCl solutions as an initial assay (Ruiz-Canada et al., 2009; Roboti and High, 2012a) to determine whether the DC2 and KCP2 proteins contribute to the association between the STT3A complex and other RAMPs (Fig. 4 A). The protein translocation channel (Sec61α) was extracted from the ribosome-containing pellet fraction as the NaCl concentration was raised (Fig. 4, A and B). STT3A complexes in WT cells showed a similar salt dependence for extraction but were less strongly associated with ribosomes than the Sec61 complex. STT3A complexes were much more soluble in cells that lacked KCP2 or both KCP2 and DC2 (Fig. 4, A and B), indicating that both DC2 and KCP2 are involved in the association between the STT3A complex and other RAMPs.

The interaction between the STT3A complex and the Sec61 complex was further analyzed using a sequential digitonin–high salt extraction procedure (Fig. 4 C) that was developed by the laboratory of W.R. Skach (Oregon Health and Science University, Portland, OR) to characterize the protein

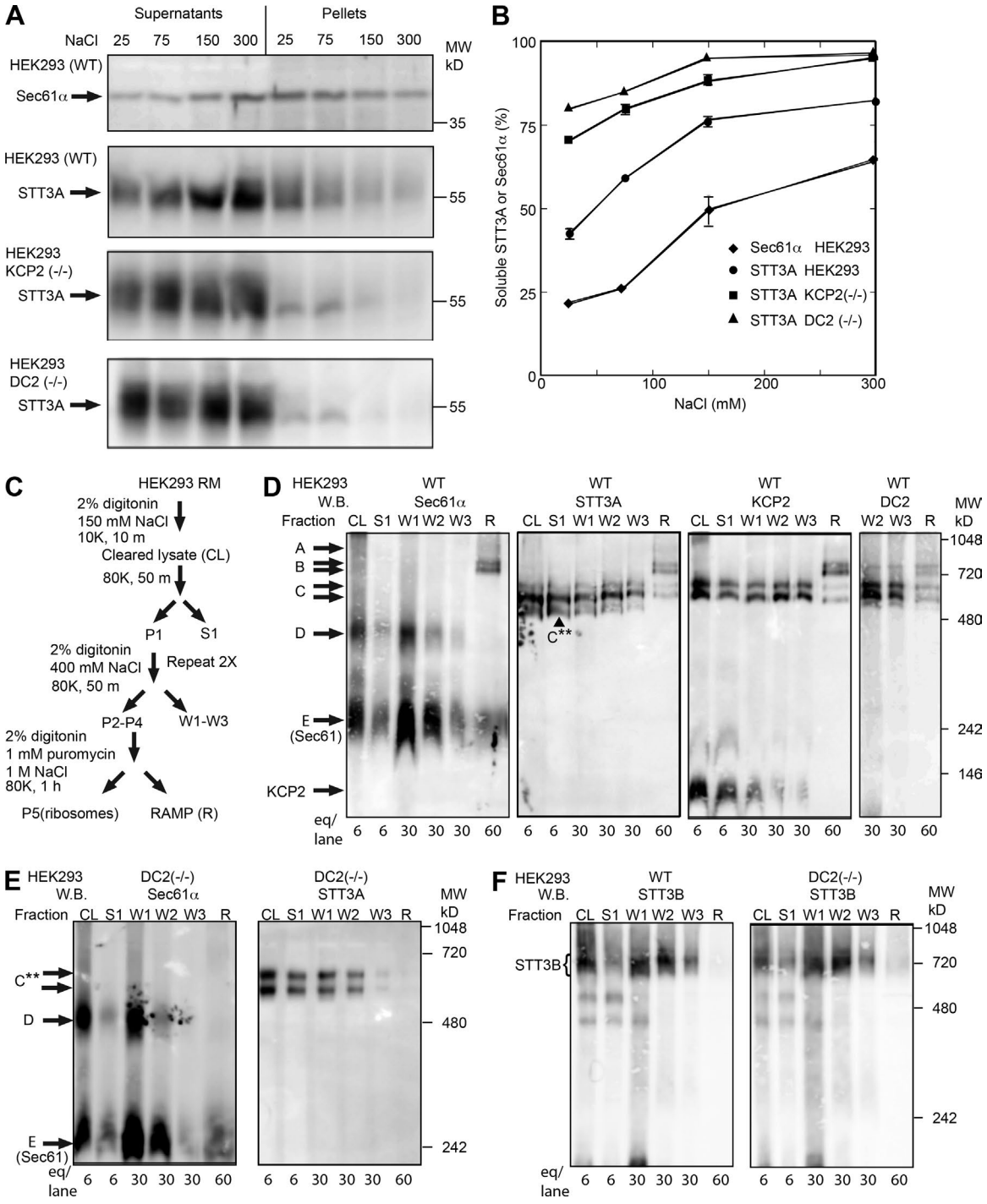

Figure 4. **Reduced association of the STT3A complex with RAMPs in *DC2*$^{-/-}$ and *KCP2*$^{-/-}$ cells.** (A) WT and mutant cells were solubilized with digitonin at different NaCl concentrations, and then centrifuged to separate detergent-soluble proteins (supernatants) from insoluble proteins (pellets). (B) Sec61α and STT3A immunoblots from A were quantified to determine the recovery of STT3A and Sec61 in the supernatant fractions. Values are the mean of two replicates; error bars indicate individual data points. (C) Diagram showing the preparation of soluble RAMP (R) complexes by sequential detergent/high salt extractions. Pellets (P1–P5) and supernatant (S1, W1–W3, R) fractions were separated by centrifugation. (D–F) BN-PAGE of fractions (CL, S1, W1–W3, R) collected during isolation of RAMPs from WT HEK293 cells (D and F) or *DC2*$^{-/-}$ cells (E and F) were analyzed by protein immunoblotting (W.B.). Early fractions (CL, S1, W1) are not depicted for the DC2 immunoblot because of nonspecific background. The amount of starting microsomes from which each gel lane is derived is expressed as equivalents (eq/lane). Labeled arrows designate the following protein complexes: A, STT3A-Sec61-TRAP; B, STT3A-Sec61; C, STT3A (470 and 500 kD); C**, STT3A complex lacking DC2 and KCP2; D, Sec61-TRAP; and E, Sec61.

complexes that interact with ER-bound ribosomes (Shibatani et al., 2005; Conti et al., 2015). The cleared cell lysate, low-salt supernatant (S1), high-salt wash fractions (400 mM NaCl; W1–W3), and final solubilized RAMP (R) fraction, obtained by releasing the ribosome with a puromycin-high salt treatment, were resolved by BN-PAGE for protein immunoblot analysis (Fig. 4, D–F). Four protein complexes (A, B, D, and E) were detected with the anti-Sec61α sera when WT HEK293

microsomes were analyzed (Fig. 4 D). Based on previous analyses (Shibatani et al., 2005; Conti et al., 2015) and confirmed here, complexes A, B, D, and E respectively correspond to the Sec61-TRAP-OST, Sec61-OST, Sec61-TRAP, and Sec61 complexes. Consistent with these assignments, complexes A and B were detected using antibodies to STT3A and KCP2 (Fig. 4 D), whereas complexes A and D were detected using an antibody specific for TRAPα (Fig. S3 A). Antibodies to STT3A, KCP2, and DC2 detected the STT3A complex as a doublet (complex C). Complex A is faint relative to complexes B and C and was not detected above background with anti-DC2 sera (Fig. 4 D). In addition to the complex C doublet, we detected a more rapidly migrating band with anti-STT3A sera in the cleared lysate (CL), S1, and W1–W3 fractions (Fig. 4 D, C** band). The C** band was not detected with anti-KCP2 or anti-DC2 sera; hence this form of the STT3A complex arises by extraction-dependent dissociation of DC2 and KCP2 during RAMP isolation. Free KCP2 migrated near the bottom of the gel (Fig. 4 D; CL, S1, and W1–W3 fractions).

When the RAMP isolation procedure was applied to *DC2*$^{-/-}$ (Fig. 4 E) or *KCP2*$^{-/-}$ (Fig. S3 B) microsomes, antisera to Sec61α recognized the Sec61-TRAP complex and Sec61 heterotrimers (complexes D and E). STT3A complexes lacking both DC2 and KCP2 were mainly recovered in the S1, W1, and W2 fractions (Fig. 4 E, C** bands), and were undetectable in the RAMP fraction, demonstrating that the DC2 protein is needed for the formation of complexes A and B. Sec61 complexes (band E) were present in all fractions including the final RAMP fraction (Fig. 4, D and E; and Fig. S3 B). Analysis of *KCP2*$^{-/-}$ cells using the RAMP isolation procedure was relatively uninformative, as the absence of KCP2 favors conversion of the C* complex lacking KCP2 into the C** complex that lacks both DC2 and KCP2. Consequently, the majority of the STT3A complex in *KCP2*$^{-/-}$ cells was recovered in the S1, W1, and W2 fractions (Fig. S3 B).

The BN-PAGE gels were also probed with antibodies to STT3B to determine whether the STT3B complex interacts with the Sec61 complex in WT or *DC2*$^{-/-}$ cells. In both cases, STT3B complexes were recovered in the wash fractions (Fig. 4 F), consistent with minimal direct interaction with the Sec61 complex (Ruiz-Canada et al., 2009).

Cytosolic and lumenal segments of DC2 are important for activity

Alignment of diverse metazoan DC2 sequences revealed a high level of sequence conservation within the TM spans and lumenal segments, as indicated by the sequence logo (Fig. 5 A). *DC2*$^{-/-}$ cells were cotransfected with a pSAP-DDKHis vector and various DC2 expression vectors to identify an epitope-tagged DC2 derivative that could restore the activity of the STT3A complex (Fig. 5 B). Because pSAP is an endogenous HEK293 glycoprotein, coexpression of DC2 and the C-terminally tagged pSAP derivative (pSAP-DDKHis) ensures that we monitor pSAP-DDKHis glycosylation exclusively in cells that express the DC2 construct. We next adjusted the quantity of the DC2 expression vector used for transfection to ensure that similar amounts of WT and mutant DC2 proteins were synthesized by the transfected cells for the experiments shown in Figs. 5 and 6. Importantly, assays of pSAP glycosylation in the transfected cells were remarkably insensitive to DC2 expression levels, primarily because assembly of STT3A complexes was saturable under these transfection conditions (Fig. S4).

Glycosylation of pSAP-DDKHis was almost completely restored by expression of untagged DC2 or N-terminally HA-tagged DC2 (HA-DC2). In contrast, the C-terminally tagged DC2 construct (DC2-HA) allowed only partial recovery of pSAP-DDKHis glycosylation, demonstrating that a C-terminal HA tag interfered with DC2 function. As expected, transfection of *DC2*$^{-/-}$ cells with KCP2-HA did not improve pSAP-DDKHis glycosylation, even though the KCP2-HA construct could restore normal glycosylation to *KCP2*$^{-/-}$ cells (Fig. S5 A). Cotransfection of *DC2*$^{-/-}$ cells with KCP2-HA plus an active DC2 construct (HA-DC2) caused an additional minor increase in pSAP-DDKHis glycosylation (Fig. 5 B). Although an increase in the length of the C-terminal tag (DC2-HA-DDKHis) did not cause a further reduction in reporter glycosylation, replacement of the entire C-terminal lumenal tail of DC2 with a DDKHis tag (HA-DC2Δ11-DDKHis) yielded an inactive form of DC2.

To identify functionally important segments of DC2, we constructed HA-DC2 deletion mutants that lack five residue segments of the cytosolic or lumenal domains (Fig. 5 A). We did not target TM spans for deletion mutagenesis, as deletion of five TM span residues should cause a folding-defective protein. Deletion of residues in the N-terminal segment caused a reduction in the ability of DC2 to promote glycosylation of pSAP-DDKHis (Fig. 5 C). Three of the five lumenal loop deletion mutants inactivated HA-DC2 (Fig. 5 C, Δ4, Δ7, and Δ8), whereas the Δ5 and Δ6 mutants caused only partial reductions in pSAP-DDKHis glycosylation (Fig. 5 C). DC2 mutants with glycosylation acceptor sites inserted into the center of the lumenal loop have partial defects in pSAP-DDKHis glycosylation (Fig. S5 B). The C-terminal deletions caused either a partial (Fig. 5 D, Δ10) or complete (Fig. 5 D, Δ9 and Δ11) inactivation of DC2. Given that the FMRMK sequence (HA-DC2 Δ9 mutant) seems to be critical for DC2 activity, individual residues in this segment were replaced with alanine. Although no single point mutation in this segment inactivated DC2, pSAP-DDKHis glycosylation was reduced by the F138A and K142A mutations (Fig. 5 D). Assay results shown in Fig. 5 (B–D) were ordered with respect to pSAP-DDKHis glycosylation (Fig. 5 E) and were found to cluster in four classes ranging between null-like activity (red symbols) and WT activity (orange symbols).

DC2 mutations interfere with complex assembly

DC2$^{-/-}$ cells expressing the HA-DC2 mutants were also analyzed by protein immunoblotting using anti-HA sera (Fig. 6 A). The intensity of the HA-DC2 signal varied between samples despite adjusting the amount of DNA used for transfection. The reduced immunoblot signal of certain HA-DC2 mutants is diagnostic of reduced protein stability, given that the immunoblot signal for GAPDH did not vary greatly between lanes.

Assembly of the DC2 mutants into the STT3A complex was evaluated by probing BN-PAGE immunoblots with anti-HA sera (Fig. 6 B). The HA-positive STT3A complexes resolved as two to three bands, consistent with heterogeneous incorporation of KCP2. Three of the HA-DC2 mutants that displayed null-like activity (Fig. 5 E, red symbols) showed fivefold or greater reduced incorporation of DC2 into the STT3A complexes (Fig. 6 B, Δ9, Δ11, HA-DC2 Δ11DDK-His). We conclude that the C-terminal tail of DC2 is critical for stable incorporation of DC2 into the STT3A complex. Reduced incorporation of C-terminal DC2 mutants into STT3A complexes likely accounts for the lower HA-DC2 protein immunoblot signal (Fig. 6 A), as

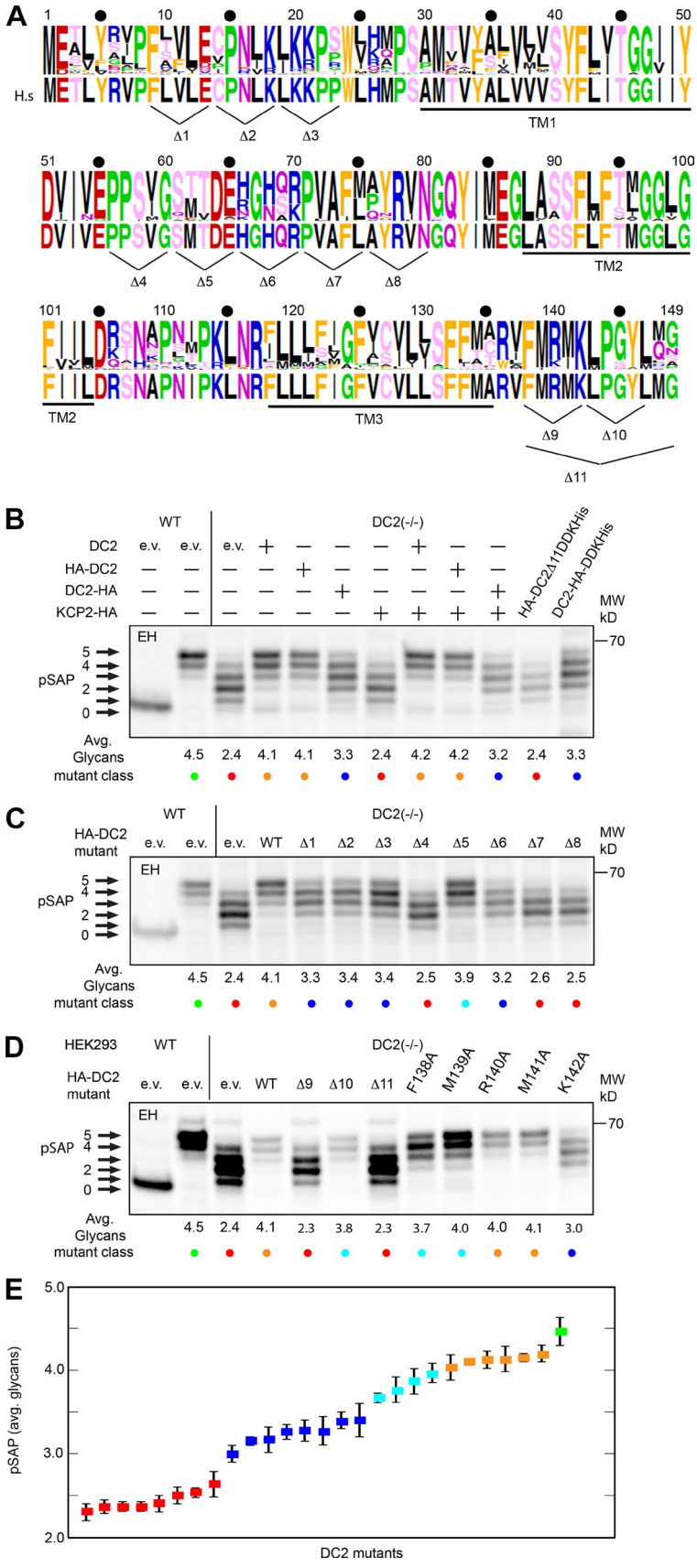

Figure 5. **Mutagenesis of DC2.** (A) A DC2 sequence logo was obtained by alignment of 44 metazoan DC2 sequences. Short N-terminal or C-terminal extensions/deletions (residues 1–3) were masked before logo construction. Residue numbers correspond to the *Homo sapiens* (H.s.) DC2 sequence, which is beneath the logo. TM spans are underlined. Residues are color coded by side chain property; letter height is proportional to frequency. Sequence logos were made using WebLogo (Crooks et al., 2017). Five residue segments in the N-terminal cytoplasmic segment (Δ1–Δ3), lumenal loop (Δ4–Δ8), and C-terminal tail (Δ9 and Δ10) of DC2 were deleted as indicated beneath the logo. (B–D) WT and *DC2*$^{-/-}$ cell lines were cotransfected with a pSAP-DDKHis expression vector plus an empty vector (e.v.), untagged DC2 and/or KCP2 expression vectors, or an epitope-tagged DC2 expression vector. 24 h after transfection, the cells were pulse labeled for 15 min. Glycoforms of pSAP-DDKHis were immunoprecipitated with anti-DDK sera. EH designates digestion with endoglycosidase H. Quantified values below gel lanes (B–D) are the mean number of glycans per protein chain as determined from three or more experiments. Labeled arrows designate the number of N-linked glycans. Colored circles designate mutant class as defined in E. (E) Assay results from B–D were ordered with respect to mean glycans/pSAP. The following color coded symbols designate the relative activity: red, <10%; blue, 30–60%; cyan 70–90%; orange, >90%; green, WT HEK293. Error bars are standard deviations calculated using three to eight determinations.

unassembled DC2 is unstable in *STT3A*$^{-/-}$ cells. Several other HA-DC2 mutants that have impaired function (Fig. 5, red, blue, and cyan symbols) show two- to threefold reductions in STT3A complex assembly (Fig. 6 B, Δ4, Δ8, M139A, K142A). In contrast, other deletions reduce DC2 activity, but do not interfere with STT3A complex assembly (Fig. 6 B, Δ1, Δ2, Δ3,

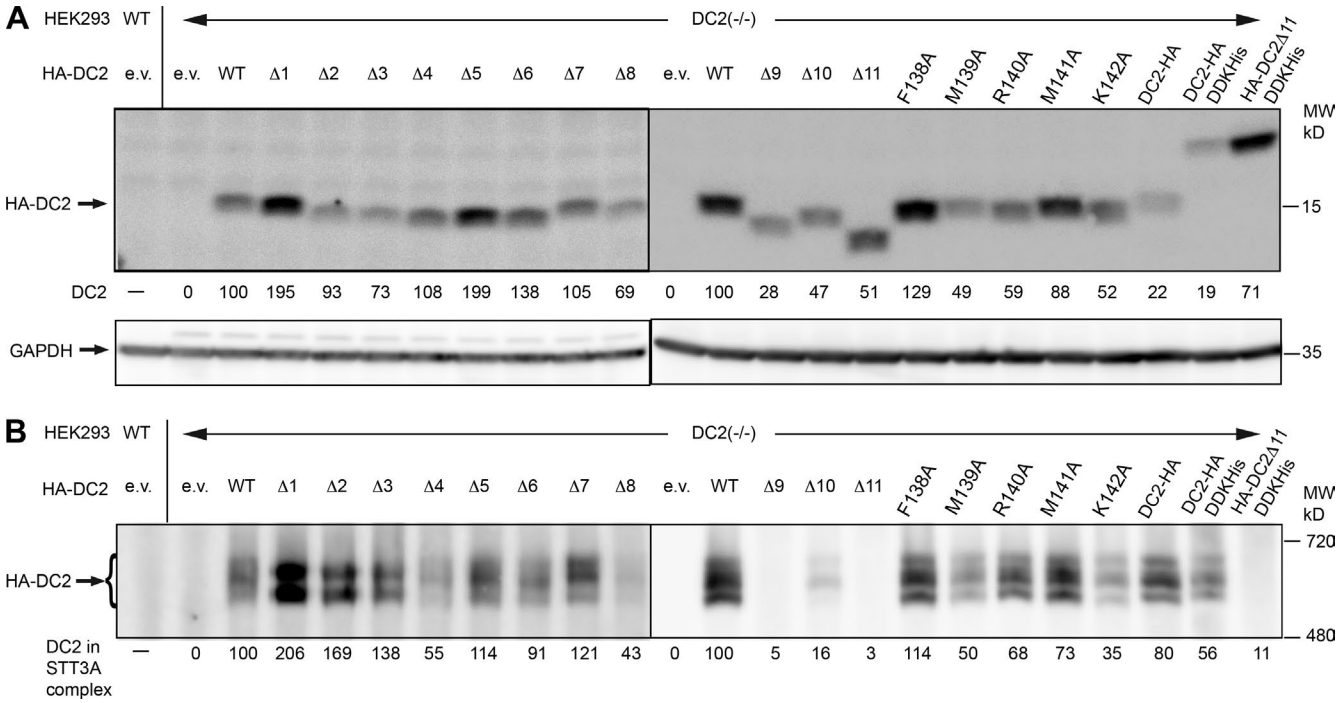

Figure 6. **Incorporation of DC2 mutants into the STT3A complex.** (A and B) Digitonin extracts from WT HEK293 or *DC2*$^{-/-}$ cells that were transfected with empty vector (e.v.) or an HA/epitope-tagged DC2 expression vector were resolved by SDS-PAGE (A) or BN-PAGE (B). Protein immunoblots were probed with anti-HA or anti-GAPDH sera to compare HA-DC2 expression (A) or HA-DC2 incorporation into the STT3A complex (B). Quantified values below gel lanes indicate the intensity of the anti-HA immunoblot signal relative to the HA-DC2 WT control lane on the same immunoblot and correspond to the mean of two determinations. Vertical lines in images designate electrophoresis on separate gels.

Δ6, Δ7). Importantly, one of the lumenal loop mutants that displays null-like activity (HA-DC2 Δ7) lacks a defect in assembly of DC2-positive STT3A complexes. We conclude that the deletions in the N-terminal cytoplasmic domain and the lumenal loop of DC2 interfere with DC2 function by mechanisms that include impacting STT3A complex assembly and interfering with the functional interaction between the STT3A complex and the Sec61 complex.

Discussion

Efficient N-glycosylation of proteins in multicellular eukaryotic organisms is essential for normal health and development, as highlighted by the growing number of gene products that cause the family of human diseases known as congenital disorders of glycosylation (CDG; Freeze et al., 2014; Scott et al., 2014). Mutations that reduce the cellular content of either OST complex cause severe forms of CDG (STT3A-CDG and STT3B-CDG; Shrimal et al., 2013a; Ghosh et al., 2017). Our previous analysis demonstrated that the STT3A complex primarily acts in a co-translational scanning manner to glycosylate acceptor sites as they emerge into the lumen of the ER, whereas the STT3B complex modifies acceptor sites that have been skipped by STT3A (Ruiz-Canada et al., 2009; Shrimal and Gilmore, 2013; Shrimal et al., 2013b; Cherepanova et al., 2014). A co-translational mode of glycosylation allows more efficient modification of acceptor sites, particularly in protein domains that rapidly acquire a folded conformation. Here, we have shown that the DC2 and KCP2 subunits of the STT3A complex are responsible for localization of the STT3A complex adjacent to the protein translocation channel to allow direct coupling between protein translocation and glycosylation.

HEK293 cells that do not express DC2 also lack KCP2 but still assemble a catalytically active STT3A complex. The DC2-deficient STT3A complex is unable to mediate efficient glycosylation of the three STT3A-dependent substrates we tested and caused an induction of the UPR pathway. Although protein glycosylation was reduced to a similar extent in *STT3A*$^{-/-}$ and *DC2*$^{-/-}$ cells, neither condition caused a complete block in glycosylation of pSAP, Tf, or pGran. Features that influence the efficiency of STT3B-dependent modification of skipped sites in proteins remain to be fully defined, but at a minimum involve disulfide bond formation kinetics (Ruiz-Canada et al., 2009) and the identity of the X residue in NXS acceptor sites (Malaby and Kobertz, 2014).

Assembly of native translocation channels in the ER

Complexes between the protein translocation channel, the TRAP complex, and 80S ribosomes were first visualized by cryoelectron microscopy (Ménétret et al., 2005, 2008). Cryo-electron tomography of native ER membranes (Pfeffer et al., 2014, 2015) revealed that the Sec61 complex is assembled into native translocation channels that include the TRAP complex and OST in defined positions relative to the Sec61 channel. The well-resolved density for OST adjacent to the Sec61 complex in these structures provides compelling evidence that OST occupies a unique site adjacent to the Sec61 channel during co-translational transport of proteins. Importantly, the molecular mass assigned to the OST complex in native protein-conducting channels is consistent with a single copy of OST (Pfeffer et al., 2014). Although the majority of Sec61 complexes (~65%) resolved by cryo-electron tomography are part of larger complexes that contain both the TRAP complex and OST (Pfeffer

et al., 2014), it is unclear whether the OST-deficient complexes that were also detected correspond to idle ribosomes docked onto the Sec61 complex (Pfeffer et al., 2015).

These structural studies did not disclose whether translocon-proximal OST was the STT3A or STT3B complex, nor does the structure have sufficient resolution to define which subunits of OST mediate the interaction with the Sec61 complex. Biochemical isolation of native translocation channels by sequential detergent extraction allows compositional analysis by BN-PAGE (Shibatani et al., 2005; Conti et al., 2015). Here, we used this approach to show that DC2 and KCP2 are necessary for the interaction between the STT3A complex and the Sec61 complex. STT3B complexes do not form biochemically detectable complexes with the Sec61 complex in the absence or presence of the DC2 protein; hence, STT3B complexes appear to occupy a more distal position even when the STT3A-Sec61 interaction is perturbed.

The enzymatically active STT3A complex that was purified from canine pancreas microsomes by classical chromatography methods lacked the DC2 and KCP2 subunits, presumably because of detergent/high salt–induced dissociation of these proteins (Kelleher et al., 2003). Here we have shown that DC2- and KCP2-deficient STT3A complexes retain normal peptide glycosylation activity. The two mobility forms of the STT3A complex observed on BN-PAGE gels led to ambiguous conclusions about the incorporation of DC2 and KCP2 into the STT3A and STT3B complexes (Roboti and High, 2012a,b). Substoichiometric binding of malectin to the STT3A complex is responsible for decreased gel mobility of the 500-kD STT3A complex relative to the 470-kD complex. DC2 and KCP2 are present in both mobility forms of the STT3A complex, but not in the diffusely migrating STT3B complex.

Analysis of STT3A- and STT3B-deficient cell lines established that the accessory subunits (DC2, KCP2, MagT1, and TUSC3) are unstable when their cognate catalytic subunit is absent, demonstrating that the catalytic subunits (STT3A or STT3B), rather than one of the shared subunits (e.g., ribophorin I), provide the specificity for incorporation of accessory subunits into the STT3A and STT3B complexes. The latter conclusion corroborates previous information concerning the direct interaction between yeast Stt3p and Ost3p (Karaoglu et al., 1997; Mueller et al., 2015).

Deletion of the C-terminal lumenally oriented tail of DC2 interfered with assembly of DC2 into the STT3A complex, as monitored by BN-PAGE; hence, the C-terminal deletion mutants were unable to rescue the glycosylation defect of the *DC2*$^{-/-}$ cell line. With the exceptions of the DC2 Δ4 and DC2 Δ8 mutants, the N-terminal and lumenal loop deletion mutants did not reduce incorporation of HA-DC2 into the STT3A complex. Although three of the lumenal loop deletion mutants (Δ4, Δ7, and Δ8) caused glycosylation defects that were null-like, all of the N-terminal deletion mutants and the two other lumenal loop deletion mutants caused partial glycosylation defects. Insertion of sequons into the center of the lumenal loop provided additional evidence that the lumenal loop is important and suggests that the interaction surface can be sterically perturbed. Together, the mutagenesis experiments indicate that multiple segments of DC2 are functionally important, and likely mediate interactions with KCP2, STT3A, and Sec61. Although not tested in the current study, we suspect that membrane-spanning segments of DC2 are also important for mediating interactions with the Sec61 complex.

Instability of KCP2 in the absence of DC2, and the dissociation of DC2 from KCP2-deficient STT3A complexes in detergent solution, prevented conclusive assessment of the relative roles of DC2 and KCP2 in mediating the OST-Sec61 interaction. However, the mild glycosylation defect displayed by *KCP2*$^{-/-}$ cells focused our attention on DC2 as the more critical component. Elimination of KCP2 reduced the recovery of the STT3A complex in ribosome-nascent chain complex pellets, suggesting that DC2 and KCP2 cooperate to mediate the association between the STT3A complex and the protein translocation channel. Because of the technical limitation of the transient transfection system, it was not feasible to determine whether a subset of the DC2 deletion mutants prevents incorporation of KCP2 into the STT3A complex; hence, this remains an open question. Notably, all DC2 deletion mutants except for DC2 Δ5 cause a more severe glycosylation defect than that displayed by the *KCP2*$^{-/-}$ cells.

The TRAP complex does not appear to be critical for the interaction between the protein translocation channel and the STT3A complex, because we can detect TRAP-deficient STT3A-Sec61 complexes by BN-PAGE. The TRAP complex and the OST complex appear to dock onto different faces of the Sec61 complex (Pfeffer et al., 2015). Nonetheless, recent evidence indicates that the TRAP complex influences the efficiency of co-translational N-glycosylation. Point mutations in the human *SSR4* gene, which encodes TRAP-δ, reduce the stable expression of the TRAP complex and cause a recently discovered form of CDG (SSR4-CDG) that is accompanied by a mild reduction in glycosylation of serum Tf, the standard CDG diagnostic marker (Losfeld et al., 2014). Cryoelectron tomographic analysis of WT and SSR4-CDG microsomes indicates that TRAP-δ is located at an interface between the TRAP complex and a lumenally exposed segment of OST (Pfeffer et al., 2017). It should be noted that reduced expression of the STT3A complex causes a more severe defect in Tf glycosylation (Shrimal et al., 2013a) than TRAP-δ deficiency. To date, CDG patients with mutations in the *DC2* or *KCP2* genes have not been described.

Genomes that encode the STT3A protein also encode DC2 and KCP2 proteins

Phylogenetic analysis of eukaryotic STT3 protein sequences revealed that an ancestral *STT3* gene was duplicated to give rise to the STT3A and STT3B proteins present in most metazoan organisms and multicellular plants (Shrimal et al., 2013b). The STT3 proteins of fungi and unicellular plants fall within the STT3B clade, suggesting that the co-translational scanning mode of glycosylation catalyzed by the STT3A complex coincided with the dramatic expansion of the glycoproteome in metazoa and multicellular plants relative to fungi (Zielinska et al., 2012). Here we have shown that DC2 and KCP2 are obligatory subunits of the STT3A complex. Consistent with this observation, the genomes of species in the genus *Caenorhabditis*, which do not encode STT3A, do not encode homologues of DC2 and KCP2. Multicellular plants, but not unicellular plants or fungi, encode DC2 and KCP2 proteins, reinforcing the notion that these complex-specific accessory subunits of the STT3A complex have an evolutionarily conserved function. The genomes of species in the genus *Dictyostelium* represent an interesting case, as they encode STT3A, DC2, KCP2, and the oxidoreductase OST3 yet do not encode STT3B. The *Dictyostelium* STT3A protein may be able to form complexes with either OST3 or DC2 and KCP2.

When initially detected in association with translocation channel–associated STT3A complexes (Shibatani et al., 2005), DC2 and KCP2 were proposed to be distant homologues of the MagT1 and TUSC3 oxidoreductases. However, the lack of a thioredoxin domain in DC2 and KCP2, and the differences in TM span number and topology, argue against such an origin.

As nascent polypeptides pass through the translocation channel at the protein synthesis elongation rate (~6 residues/s), a co-translational scanning mechanism allows efficient glycosylation of acceptor sites before the formation of disulfide bonds and tertiary structure. DC2- and KCP2-dependent localization of the STT3A complex adjacent to the protein translocation channel provides a mechanism to ensure that OST is in position to scan the nascent polypeptide for acceptor sites as soon as the channel is gated by the signal sequence.

Materials and methods

Cell culture, transfection, and immunoblotting

HEK293 cells were cultured in 10-cm^2 dishes at 37°C in DMEM (Gibco), 10% FBS with 100 U/ml penicillin, and 100 µg/ml streptomycin. Cells were seeded at 80% confluence, transfected with vectors using Lipofectamine 2000 according to a protocol from the manufacturer (Invitrogen), and processed after 24 h.

Expression of STT3A, STT3B, ribophorin I, DC2, KCP2, malectin, Sec61α, GAPDH, and BiP was analyzed by protein immunoblotting as described previously (Ruiz-Canada et al., 2009). Rabbit antibody specific for STT3B was raised against the recombinantly expressed 73 N-terminal residues of human STT3B as described (Ruiz-Canada et al., 2009). Rabbit polyclonal antibody against STT3A was raised against a synthetic peptide corresponding to the C terminus of human STT3A (residues 693–705) as described (Kelleher et al., 2003). Rabbit antibody to ribophorin I (RIC6; Yu et al., 1990) was raised against residues 564–583 of rat ribophorin I. Rabbit anti–saposin D was raised against recombinantly expressed human saposin D (residues 410–487 of human pSAP) as described (Klein et al., 1994). Rabbit anti-Sec61α antibody was raised against a synthetic peptide corresponding to residues 463–476 of human Sec61α as described previously (Song et al., 2000). Rabbit anti–TRAP-α antibody was raised against a synthetic peptide corresponding to the 15 C-terminal residues of canine TRAP-α (Prehn et al., 1990) and was provided by T. Rapoport (Harvard Medical School, Boston, MA). Mouse monoclonal antibody to GAPDH (60004) was obtained from Proteintech Group. Mouse monoclonal anti-BiP (610978) was from BD Biosciences. Goat polyclonal antisera specific for pGran (AF2420) and SHBG (VFJ01) were purchased from R&D Systems. Rabbit polyclonal anti-malectin (SAB4200245) and mouse monoclonal anti-DDK (F3165 anti-FLAG M2) were obtained from Sigma-Aldrich. Rabbit polyclonal anti-DC2 antibody (PA5-34060) was purchased from Thermo Fisher Scientific. Rabbit polyclonal anti-KCP2 antibody (LS-C187087) was obtained from LifeSpan Biosciences. Mouse monoclonal anti-HA antibody (11867423001) was from Roche.

Digitonin extracts for protein immunoblotting

HEK293 cells were washed twice with PBS and lysed at 4°C in buffer containing 20 mM Tris-Cl, pH 7.4, 150 mM NaCl, 2% digitonin, 5 mM $MgCl_2$, 3 mM $MnCl_2$, DNase, and 1× protease inhibitor cocktail (PIC; Kelleher et al. [1992]). The cell extracts were passed through a 22-gauge syringe and incubated on ice for 30 min. The digitonin extracts were centrifuged for 10 min at 13,000 rpm in a benchtop centrifuge to remove insoluble material. The supernatant was collected and analyzed by protein immunoblotting.

Generation of HEK293-derived cell lines

The CRISPR/Cas9 system was used to generate HEK293-derived cell lines using the protocols described by the laboratory of F. Zhang (McGovern Institute for Brain Research at MIT, Cambridge, MA; Ran et al., 2013). Design of the guide RNAs was achieved using the CRISPR design tool (Massachusetts Institute of Technology, 2014; Hsu et al., 2013). Guide oligonucleotide primers were cloned into the vector pSpCas9(BB)-2A-GFP (plasmid ID PX458; Addgene) and transfected into HEK293 cells. Cells were collected by trypsinization 24 h after transfection and subjected to FACS using a BD FACSVantage DV1 Cell Sorter to obtain GFP-positive cells that were plated as single cells into 96-well plates. After 2 wk, surviving colonies were isolated and expanded. Genomic DNA was isolated from potential colonies with Quick Extract Solution (EpiCentre). DNA flanking the CRISPR target sites was amplified by PCR using Phusion (New England BioLabs) and cloned into pJet1.2 vector (Thermo Fisher Scientific) for DNA sequencing. DNA sequences were aligned to the WT DNA to detect insertions or deletions. Total cell extracts were prepared from colonies for protein immunoblot analysis using antibodies specific for the targeted protein. The *STT3A*$^{-/-}$ and *STT3B*$^{-/-}$ HEK293-derived cell lines were described previously (Cherepanova and Gilmore, 2016).

Pulse-chase radiolabeling and immunoprecipitation

The procedures for pulse labeling and pulse-chase labeling of cells and immunoprecipitation of glycoproteins have been described (Shrimal and Gilmore, 2013; Shrimal et al., 2013b). The pulse and chase intervals were as follows: pSAP, pGran, and Tf, 15-min pulse; SHBG, 5-min pulse/20-min chase. The glycoprotein substrates were immunoprecipitated with anti-DDK, anti-SapD, anti-Gran, and anti-SHBG sera and then resolved by SDS-PAGE. As indicated, immunoprecipitated proteins were digested with endoglycosidase H (New England BioLabs). Dry gels were exposed to a phosphor screen, scanned in Typhoon FLA 9000 (GE Healthcare), and quantified using AlphaEaseFC.

Expression vectors and siRNA treatments

A full-length human *DC2* verified clone (MHS 6278–202839922) was purchased from GE Healthcare and amplified by PCR to append an HA coding sequence at either the N terminus or the C terminus. The amplification products were then cloned into a pCMV6-AC-DDK-His vector (OriGene) with a stop codon inserted upstream of the DDK-His coding sequence. A stop codon was then introduced into the DC2-HA expression vector to generate the untagged DC2 expression vector. HA-DC2 point mutants and deletion mutants were generated using standard site-directed mutagenesis, and all clones were sequenced to confirm the desired mutations. The DC2 glycosylation site mutants were constructed by replacing DC2 residues 68–71 (PQRP) with NNTS or residues 71–73 (PVA) with NVT.

DC2$^{-/-}$ cells (60-mm dish) were transfected initially with 4 µg HA-tagged DC2 expression plasmid, and cells were pulse labeled for 15 min with ^{35}S Translabel after 24 h of culture. Newly synthesized DC2 protein was recovered by immunoprecipitation with anti-HA sera and resolved by SDS-PAGE. The quantified values of radiolabeled HA-tagged DC2 were used to adjust the amount of DC2 expression vector used for subsequent experiments to achieve similar amounts of newly synthesized HA-DC2. *DC2*$^{-/-}$ cells were transfected with equal amounts of total plasmid (HA-DC2 vector + pSAP-DDKHis reporter + empty vector). One set of transfected cell dishes was pulse labeled for the pSAP glycosylation assays, and a parallel set of plates was solubilized in digitonin for immunoblot analysis of HA-DC2 resolved by SDS-PAGE and BN-PAGE. Differences in HA-immunoblot signals for the HA-DC2 mutants (Fig. 6 A) reflect differences in the in vivo stability of the HA-DC2 mutants.

A KCP2 expression construct was purchased from the RNAi Core facility at University of Massachusetts Medical School (MGC-35430). An HA tag coding sequence was introduced before the C-terminal KKRN sequence, which functions as an ER retention motif of KCP2 (Roboti and High, 2012a). The KCP2/HA/stop codon expression construct was cloned into the pCMV6-AC-DDK-His vector. The KCP2 glycosylation site mutant was constructed by inserting the sequence EHGHQRPVNSTAFLAYRVN between residues 28 and 29 of KCP2, where the underlined residues correspond to the glycosylation site.

The siRNA for STT3A (Ruiz-Canada et al., 2009; Shrimal et al., 2013b) and KCP2 (5′-UGGUUGGUCUGUACUACAUTT3′; Roboti and High, 2012b) were characterized previously and were obtained from Dharmacon/Thermo Fisher Scientific). Silencer select predesigned siRNAs were purchased from Ambion for *DC2* (s33884; 5′-CCAAGUGUCGGUUCUAUGATT-3′) and malectin (s18843; 5′-CAG GGAAACUCUACAUUGATT-3′). Negative control siRNA (1027310) was purchased from Qiagen.

STT3B$^{-/-}$ cells were seeded at 20% confluence and grown for 24 h before transfection with 60 nM dsRNA and Lipofectamine RNAiMAX in OptiMEM using protocols from Life Technologies. After 48 h, cells were subjected to a second siRNA transfection (40 nm) with or without a reporter plasmid using Lipofectamine 2000 and were assayed after 24 h. A malectin-HA expression vector was provided by M. Molinari (Institute for Research in Biomedicine, Bellinzona, Switzerland). Malectin siRNA were transfected at 75 nM, and cells were assayed after 72 h.

Differential solubilization of OST complexes in digitonin-NaCl solutions

HEK293 or mutant cells were solubilized at 4°C with 1 ml of 20 mM Tris-Cl, pH 7.4, 1.5% digitonin, 5 mM $MgCl_2$, 3 mM $MnCl_2$, 12% glycerol, 1 mM DTT, DNase, 1× PIC, and 1 mM cycloheximide adjusted to 25, 75, 150, or 300 mM NaCl. After 30-min incubation on ice, the cell extracts were centrifuged for 20 min at 270,000 g_{av} in a TLA-100.4 rotor. Supernatants were collected, and the pellet was solubilized in 50 mM Tris-Cl and 0.5% SDS. Supernatant and pellet fractions derived from equal amounts of cells were loaded for SDS-PAGE and immunoblotting.

Microsome preparation

20 confluent 100-mm plates of cells were trypsinized and centrifuged at 600 *g* for 5 min. The cell pellets were washed twice with Ca^{2+}, Mg^{2+}-free DPBS. Cells were incubated in buffer A (10 mM Hepes, pH 7.8, 1 mM EGTA, 25 mM KCl, and 1× PIC) for 20 min at 4°C and centrifuged at 600 *g* for 5 min. The pellet was resuspended in buffer A adjusted to 250 mM sucrose using 20 strokes of a dounce homogenizer. The suspension was centrifuged at 1,000 *g* for 10 min, and the resulting supernatant was recentrifuged at 12,000 *g* for 15 min. The postmitochondrial supernatant was centrifuged at 417,000 g_{av} in a TLA-100.4 rotor for 1 h to pellet microsomal membranes, which were resuspended in 50 mM triethanolamine, pH 7.5, 250 mM sucrose, and 1 mM DTT.

RAMP isolation and BN-PAGE analysis

The isolation of soluble RAMP complexes for BN-PAGE analysis used a procedure described by the Skach laboratory (Shibatani et al., 2005; Conti et al., 2015). Microsomes from WT and mutant HEK293 cells were suspended in buffer B (20 mM Tris-Cl, pH 7.4, 5 mM $Mg(OAc)_2$, 3 mM $MnCl_2$, 1 mM DTT, 1× PIC, 2% digitonin, 12% glycerol) adjusted to 150 mM NaCl for 30 min. The detergent-solubilized microsomes were centrifuged at 10,000 rpm for 10 min, and the resulting CL was recentrifuged at 80,000 rpm for 50 min to obtain a supernatant fraction (S1) and an initial ribosome-membrane protein pellet (P1). The P1 fraction was resuspended in buffer B adjusted to 400 mM NaCl and centrifuged to obtain a supernatant fraction (W1) and a pellet fraction (P2) that was subjected to two more high-salt wash steps. The washed pellet (P4) corresponds to ribosome-nascent chain complexes and associated RAMP proteins. The RAMP complexes were eluted by incubating the P4 fraction in 2 mM puromycin, 2 mM GTP, 1 M NaCl, 100 mM Hepes, pH 7.8, 15 mM $Mg(OAc)_2$, 5 mM DTT, 1× PIC, 1% digitonin, and 15% glycerol at 4°C for 45 min followed by ultracentrifugation to pellet the ribosomes. Digitonin extracts of cells and the fractions obtained during the RAMP isolation (CL, S1, W1–W3, and R) were analyzed by BN-PAGE as described previously (Shrimal and Gilmore, 2015).

OST assay

OST activity was measured using a fluorescently labeled hexapeptide (5′-TAMRA-GNSTVT-NH_2) containing the underlined glycosylation site as the acceptor substrate (Kohda et al., 2007) and a bovine Dol-PP-OS preparation that was purified and characterized as described previously (Kelleher et al., 2001). Aliquots of Dol-PP-OSs in $CHCl_3$/CH_3OH/H_2O (10:10:3) were transferred to a microfuge tube and dried in a SpeedVac concentrator. The dried Dol-PP-OS substrate was dissolved in 7.5 µl DMSO by vortexing, as Dol-PP-OS is insoluble in digitonin. The Dol-PP-OS solution was diluted with 31.5 µl of 8% glycerol, 2.14 mM egg phosphatidylcholine, 0.3 mM $MnCl_2$, 0.2 mM EDTA, and 48 mM Tris-Cl, pH 7.4, followed by the addition of 5 µl assay buffer (200 mM Tris-Cl, pH 7.4, 40 mM NaCl, 100 mM $MnCl_2$, 50 mM $Mg(OAc)_2$, 1% digitonin, 8 mM DTT, and 10 mM deoxynojirimycin). 100 µg microsomes in 7.5 µl of 50 mM triethanolamine-acetate, pH 7.5, 250 mM sucrose, and 1 mM DTT were added, and the reaction was preincubated at 30°C for 5 min followed by addition of the fluorescent acceptor peptide at 5 µM concentration to obtain a final assay volume of 52.5 µl. The OST assays were incubated for 2 h at 30°C and terminated by the addition of 4× SDS sample buffer.

The sample was heated at 55°C for 20 min and loaded onto a Tricine SDS-PAGE gel consisting of a 16% resolving gel with 6 M urea, a 10% spacer gel, and a 4% stacking gel (Gerber et al., 2013). Fluorescent bands for the peptide substrate and the glycopeptide product were visualized using a Typhoon FLA 9000 (GE Healthcare) at 532 nm.

Online supplemental material

Fig. S1 shows DNA sequences of the indel mutations created in the DC2 and KCP2 genes. Fig. S2 A presents evidence for a direct interaction between DC2 and KCP2. Fig. S2 (B and C) presents evidence that malectin, DC2, and KCP2 are subunits of the STT3A complex. Fig. S3 shows BN-PAGE protein immunoblot analysis of fractions obtained in RAMP preparations of HEK293 cells and *KCP2*$^{-/-}$ cells. Fig. S4 presents evidence that the pSAP-DDKHis glycosylation assays shown in Fig. 5 are insensitive to threefold differences in HA-DC2 expression because of saturation of STT3A complex assembly. Fig. S5 A shows that expression of the KCP2-HA construct restores glycosylation activity to *KCP2*$^{-/-}$ cells. Fig. S5 B shows that HA-DC2 mutants with N-glycosylation sites in the lumenal loop are compromised in DC2 activity. Table S1 lists the target sequences in the *DC2* and *KCP2* genes used for CRISPR/Cas9 gene editing. Table S2 lists the potential off-target sequences for the DC2 and KCP2 sgRNAs analyzed in Fig. S1 B.

Acknowledgments

The authors thank Maurizio Molinari for the malectin-HA expression construct and Tom Rapoport for the anti–TRAP-α sera.

Research reported in this publication was supported by the National Institute of General Medical Sciences of the National Institutes of Health under award number GM43768.

The authors declare no competing financial interests.

Author contributions: R. Gilmore and S. Shrimal conceived the study and designed experiments. S. Shrimal and N.A. Cherepanova performed experiments. All authors analyzed results and wrote the manuscript.

Submitted: 24 February 2017
Revised: 29 June 2017
Accepted: 27 July 2017

References

Chen, W., J. Helenius, I. Braakman, and A. Helenius. 1995. Cotranslational folding and calnexin binding during glycoprotein synthesis. *Proc. Natl. Acad. Sci. USA.* 92:6229–6233. http://dx.doi.org/10.1073/pnas.92.14.6229

Cherepanova, N.A., and R. Gilmore. 2016. Mammalian cells lacking either the cotranslational or posttranslocational oligosaccharyltransferase complex display substrate-dependent defects in asparagine linked glycosylation. *Sci. Rep.* 6:20946. http://dx.doi.org/10.1038/srep20946

Cherepanova, N.A., S. Shrimal, and R. Gilmore. 2014. Oxidoreductase activity is necessary for N-glycosylation of cysteine-proximal acceptor sites in glycoproteins. *J. Cell Biol.* 206:525–539. http://dx.doi.org/10.1083/jcb.201404083

Cheung, J.C., and R.A. Reithmeier. 2007. Scanning N-glycosylation mutagenesis of membrane proteins. *Methods.* 41:451–459. http://dx.doi.org/10.1016/j.ymeth.2006.10.002

Conti, B.J., P.K. Devaraneni, Z. Yang, L.L. David, and W.R. Skach. 2015. Cotranslational stabilization of Sec62/63 within the ER Sec61 translocon is controlled by distinct substrate-driven translocation events. *Mol. Cell.* 58:269–283. http://dx.doi.org/10.1016/j.molcel.2015.02.018

Crooks, G.E., G. Hon, J.-M. Chandonia, and S.E. Brenner. 2017. WebLogo. Available at: http://weblogo.berkeley.edu/logo.cgi. Accessed August 3, 2015.

Freeze, H.H., J.X. Chong, M.J. Bamshad, and B.G. Ng. 2014. Solving glycosylation disorders: Fundamental approaches reveal complicated pathways. *Am. J. Hum. Genet.* 94:161–175. http://dx.doi.org/10.1016/j.ajhg.2013.10.024

Gerber, S., C. Lizak, G. Michaud, M. Bucher, T. Darbre, M. Aebi, J.L. Reymond, and K.P. Locher. 2013. Mechanism of bacterial oligosaccharyltransferase: In vitro quantification of sequon binding and catalysis. *J. Biol. Chem.* 288:8849–8861. http://dx.doi.org/10.1074/jbc.M112.445940

Ghosh, A., J. Urquhart, S. Daly, A. Ferguson, D. Scotcher, A.A.M. Morris, and J. Clayton-Smith. 2017. Phenotypic heterogeneity in a congenital disorder of glycosylation caused by mutations in STT3A. *J. Child Neurol.* 32:560–565. http://dx.doi.org/10.1177/0883073817696816

Hsu, P.D., D.A. Scott, J.A. Weinstein, F.A. Ran, S. Konermann, V. Agarwala, Y. Li, E.J. Fine, X. Wu, O. Shalem, et al. 2013. DNA targeting specificity of RNA-guided Cas9 nucleases. *Nat. Biotechnol.* 31:827–832. http://dx.doi.org/10.1038/nbt.2647

Karaoglu, D., D.J. Kelleher, and R. Gilmore. 1997. The highly conserved Stt3 protein is a subunit of the yeast oligosaccharyltransferase and forms a subcomplex with Ost3p and Ost4p. *J. Biol. Chem.* 272:32513–32520. http://dx.doi.org/10.1074/jbc.272.51.32513

Kelleher, D.J., G. Kreibich, and R. Gilmore. 1992. Oligosaccharyltransferase activity is associated with a protein complex composed of ribophorins I and II and a 48 kd protein. *Cell.* 69:55–65. http://dx.doi.org/10.1016/0092-8674(92)90118-V

Kelleher, D.J., D. Karaoglu, and R. Gilmore. 2001. Large-scale isolation of dolichol-linked oligosaccharides with homogeneous oligosaccharide structures: Determination of steady-state dolichol-linked oligosaccharide compositions. *Glycobiology.* 11:321–333. http://dx.doi.org/10.1093/glycob/11.4.321

Kelleher, D.J., D. Karaoglu, E.C. Mandon, and R. Gilmore. 2003. Oligosaccharyltransferase isoforms that contain different catalytic STT3 subunits have distinct enzymatic properties. *Mol. Cell.* 12:101–111. http://dx.doi.org/10.1016/S1097-2765(03)00243-0

Klein, A., M. Henseler, C. Klein, K. Suzuki, K. Harzer, and K. Sandhoff. 1994. Sphingolipid activator protein D (sap-D) stimulates the lysosomal degradation of ceramide in vivo. *Biochem. Biophys. Res. Commun.* 200:1440–1448. http://dx.doi.org/10.1006/bbrc.1994.1612

Kohda, D., M. Yamada, M. Igura, J. Kamishikiryo, and K. Maenaka. 2007. New oligosaccharyltransferase assay method. *Glycobiology.* 17:1175–1182. http://dx.doi.org/10.1093/glycob/cwm087

Kowarik, M., S. Küng, B. Martoglio, and A. Helenius. 2002. Protein folding during cotranslational translocation in the endoplasmic reticulum. *Mol. Cell.* 10:769–778. http://dx.doi.org/10.1016/S1097-2765(02)00685-8

Lin, Y.C., M. Boone, L. Meuris, I. Lemmens, N. Van Roy, A. Soete, J. Reumers, M. Moisse, S. Plaisance, R. Drmanac, et al. 2014. Genome dynamics of the human embryonic kidney 293 lineage in response to cell biology manipulations. *Nat. Commun.* 5:4767. http://dx.doi.org/10.1038/ncomms5767

Lizak, C., S. Gerber, S. Numao, M. Aebi, and K.P. Locher. 2011. X-ray structure of a bacterial oligosaccharyltransferase. *Nature.* 474:350–355. http://dx.doi.org/10.1038/nature10151

Losfeld, M.E., B.G. Ng, M. Kircher, K.J. Buckingham, E.H. Turner, A. Eroshkin, J.D. Smith, J. Shendure, D.A. Nickerson, M.J. Bamshad, University of Washington Center for Mendelian Genomics, H.H. Freeze. 2014. A new congenital disorder of glycosylation caused by a mutation in SSR4, the signal sequence receptor 4 protein of the TRAP complex. *Hum. Mol. Genet.* 23:1602–1605.

Malaby, H.L., and W.R. Kobertz. 2014. The middle X residue influences cotranslational N-glycosylation consensus site skipping. *Biochemistry.* 53:4884–4893. http://dx.doi.org/10.1021/bi500681p

Massachusetts Institute of Technology. 2014. CRISPR Design. Available at: http://www.crispr.mit.edu (accessed August 28, 2014).

Matsumoto, S., A. Shimada, J. Nyirenda, M. Igura, Y. Kawano, and D. Kohda. 2013. Crystal structures of an archaeal oligosaccharyltransferase provide insights into the catalytic cycle of N-linked protein glycosylation. *Proc. Natl. Acad. Sci. USA.* 110:17868–17873. http://dx.doi.org/10.1073/pnas.1309777110

Ménétret, J.F., R.S. Hegde, S.U. Heinrich, P. Chandramouli, S.J. Ludtke, T.A. Rapoport, and C.W. Akey. 2005. Architecture of the ribosome-channel complex derived from native membranes. *J. Mol. Biol.* 348:445–457. http://dx.doi.org/10.1016/j.jmb.2005.02.053

Ménétret, J.F., R.S. Hegde, M. Aguiar, S.P. Gygi, E. Park, T.A. Rapoport, and C.W. Akey. 2008. Single copies of Sec61 and TRAP associate with a nontranslating mammalian ribosome. *Structure.* 16:1126–1137. http://dx.doi.org/10.1016/j.str.2008.05.003

Mueller, S., A. Wahlander, N. Selevsek, C. Otto, E.M. Ngwa, K. Poljak, A.D. Frey, M. Aebi, and R. Gauss. 2015. Protein degradation corrects for imbalanced subunit stoichiometry in OST complex assembly. *Mol. Biol. Cell.* 26:2596–2608. http://dx.doi.org/10.1091/mbc.E15-03-0168

Nilsson, I.M., and G. von Heijne. 1993. Determination of the distance between the oligosaccharyltransferase active site and the endoplasmic reticulum membrane. *J. Biol. Chem.* 268:5798–5801.

Nilsson, I., D.J. Kelleher, Y. Miao, Y. Shao, G. Kreibich, R. Gilmore, G. von Heijne, and A.E. Johnson. 2003. Photocross-linking of nascent chains to the STT3 subunit of the oligosaccharyltransferase complex. *J. Cell Biol.* 161:715–725. http://dx.doi.org/10.1083/jcb.200301043

Pfeffer, S., J. Dudek, M. Gogala, S. Schorr, J. Linxweiler, S. Lang, T. Becker, R. Beckmann, R. Zimmermann, and F. Förster. 2014. Structure of the mammalian oligosaccharyl-transferase complex in the native ER protein translocon. *Nat. Commun.* 5:3072. http://dx.doi.org/10.1038/ncomms4072

Pfeffer, S., L. Burbaum, P. Unverdorben, M. Pech, Y. Chen, R. Zimmermann, R. Beckmann, and F. Förster. 2015. Structure of the native Sec61 protein-conducting channel. *Nat. Commun.* 6:8403. http://dx.doi.org/10.1038/ncomms9403

Pfeffer, S., J. Dudek, M. Schaffer, B.G. Ng, S. Albert, J.M. Plitzko, W. Baumeister, R. Zimmermann, H.H. Freeze, B.D. Engel, and F. Förster. 2017. Dissecting the molecular organization of the translocon-associated protein complex. *Nat. Commun.* 8:14516. http://dx.doi.org/10.1038/ncomms14516

Prehn, S., J. Herz, E. Hartmann, T.V. Kurzchalia, R. Frank, K. Roemisch, B. Dobberstein, and T.A. Rapoport. 1990. Structure and biosynthesis of the signal-sequence receptor. *Eur. J. Biochem.* 188:439–445. http://dx.doi.org/10.1111/j.1432-1033.1990.tb15421.x

Qin, S.Y., D. Hu, K. Matsumoto, K. Takeda, N. Matsumoto, Y. Yamaguchi, and K. Yamamoto. 2012. Malectin forms a complex with ribophorin I for enhanced association with misfolded glycoproteins. *J. Biol. Chem.* 287:38080–38089. http://dx.doi.org/10.1074/jbc.M112.394288

Ran, F.A., P.D. Hsu, J. Wright, V. Agarwala, D.A. Scott, and F. Zhang. 2013. Genome engineering using the CRISPR-Cas9 system. *Nat. Protoc.* 8:2281–2308. http://dx.doi.org/10.1038/nprot.2013.143

Roboti, P., and S. High. 2012a. Keratinocyte-associated protein 2 is a bona fide subunit of the mammalian oligosaccharyltransferase. *J. Cell Sci.* 125:220–232. http://dx.doi.org/10.1242/jcs.094599

Roboti, P., and S. High. 2012b. The oligosaccharyltransferase subunits OST48, DAD1 and KCP2 function as ubiquitous and selective modulators of

mammalian N-glycosylation. *J. Cell Sci.* 125:3474–3484. http://dx.doi.org/10.1242/jcs.103952

Ruiz-Canada, C., D.J. Kelleher, and R. Gilmore. 2009. Cotranslational and posttranslational N-glycosylation of polypeptides by distinct mammalian OST isoforms. *Cell.* 136:272–283. http://dx.doi.org/10.1016/j.cell.2008.11.047

Schallus, T., C. Jaeckh, K. Fehér, A.S. Palma, Y. Liu, J.C. Simpson, M. Mackeen, G. Stier, T.J. Gibson, T. Feizi, et al. 2008. Malectin: A novel carbohydrate-binding protein of the endoplasmic reticulum and a candidate player in the early steps of protein N-glycosylation. *Mol. Biol. Cell.* 19:3404–3414. http://dx.doi.org/10.1091/mbc.E08-04-0354

Schallus, T., K. Fehér, U. Sternberg, V. Rybin, and C. Muhle-Goll. 2010. Analysis of the specific interactions between the lectin domain of malectin and diglucosides. *Glycobiology.* 20:1010–1020. http://dx.doi.org/10.1093/glycob/cwq059

Scott, K., T. Gadomski, T. Kozicz, and E. Morava. 2014. Congenital disorders of glycosylation: New defects and still counting. *J. Inherit. Metab. Dis.* 37:609–617. http://dx.doi.org/10.1007/s10545-014-9720-9

Shibatani, T., L.L. David, A.L. McCormack, K. Frueh, and W.R. Skach. 2005. Proteomic analysis of mammalian oligosaccharyltransferase reveals multiple subcomplexes that contain Sec61, TRAP, and two potential new subunits. *Biochemistry.* 44:5982–5992. http://dx.doi.org/10.1021/bi047328f

Shrimal, S., and R. Gilmore. 2013. Glycosylation of closely spaced acceptor sites in human glycoproteins. *J. Cell Sci.* 126:5513–5523. http://dx.doi.org/10.1242/jcs.139584

Shrimal, S., and R. Gilmore. 2015. Reduced expression of the oligosaccharyltransferase exacerbates protein hypoglycosylation in cells lacking the fully assembled oligosaccharide donor. *Glycobiology.* 25:774–783. http://dx.doi.org/10.1093/glycob/cwv018

Shrimal, S., B.G. Ng, M.E. Losfeld, R. Gilmore, and H.H. Freeze. 2013a. Mutations in STT3A and STT3B cause two congenital disorders of glycosylation. *Hum. Mol. Genet.* 22:4638–4645. http://dx.doi.org/10.1093/hmg/ddt312

Shrimal, S., S.F. Trueman, and R. Gilmore. 2013b. Extreme C-terminal sites are posttranslocationally glycosylated by the STT3B isoform of the OST. *J. Cell Biol.* 201:81–95. http://dx.doi.org/10.1083/jcb.201301031

Siepen, J.A., E.J. Keevil, D. Knight, and S.J. Hubbard. 2007. Prediction of missed cleavage sites in tryptic peptides aids protein identification in proteomics. *J. Proteome Res.* 6:399–408. http://dx.doi.org/10.1021/pr060507u

Song, W., D. Raden, E.C. Mandon, and R. Gilmore. 2000. Role of Sec61alpha in the regulated transfer of the ribosome-nascent chain complex from the signal recognition particle to the translocation channel. *Cell.* 100:333–343. http://dx.doi.org/10.1016/S0092-8674(00)80669-8

Wacker, M., D. Linton, P.G. Hitchen, M. Nita-Lazar, S.M. Haslam, S.J. North, M. Panico, H.R. Morris, A. Dell, B.W. Wren, and M. Aebi. 2002. N-linked glycosylation in *Campylobacter jejuni* and its functional transfer into *E. coli*. *Science.* 298:1790–1793. http://dx.doi.org/10.1126/science.298.5599.1790

Whitley, P., I.M. Nilsson, and G. von Heijne. 1996. A nascent secretory protein may traverse the ribosome/endoplasmic reticulum translocase complex as an extended chain. *J. Biol. Chem.* 271:6241–6244. http://dx.doi.org/10.1074/jbc.271.11.6241

Yan, Q., and W.J. Lennarz. 2002. Studies on the function of oligosaccharyl transferase subunits. Stt3p is directly involved in the glycosylation process. *J. Biol. Chem.* 277:47692–47700. http://dx.doi.org/10.1074/jbc.M208136200

Yu, Y.H., D.D. Sabatini, and G. Kreibich. 1990. Antiribophorin antibodies inhibit the targeting to the ER membrane of ribosomes containing nascent secretory polypeptides. *J. Cell Biol.* 111:1335–1342. http://dx.doi.org/10.1083/jcb.111.4.1335

Zielinska, D.F., F. Gnad, K. Schropp, J.R. Wiśniewski, and M. Mann. 2012. Mapping N-glycosylation sites across seven evolutionarily distant species reveals a divergent substrate proteome despite a common core machinery. *Mol. Cell.* 46:542–548. http://dx.doi.org/10.1016/j.molcel.2012.04.031